Inferring Charge-Noise Source Locations from Correlations in Spin Qubits

J. S. Rojas-Arias,[1,*] A. Noiri,[2] J. Yoneda,[3] P. Stano,[1,4] T. Nakajima,[2] K. Takeda,[2,†] T. Kobayashi,[1] G. Scappucci,[5] S. Tarucha,[2,1,†] and D. Loss[1,6]
[1]RIKEN, Center for Quantum Computing (RQC), Wako-shi, Saitama 351-0198, Japan
[2]RIKEN, Center for Emergent Matter Science (CEMS), Wako-shi, Saitama 351-0198, Japan
[3]Department of Advanced Materials Science, University of Tokyo, Kashiwa, Chiba 277-8561, Japan
[4]Slovak Academy of Sciences, Institute of Physics, 845 11 Bratislava, Slovakia
[5]QuTech and Kavli Institute of Nanoscience, Delft University of Technology, Lorentzweg 1, 2628 CJ Delft, Netherlands
[6]Department of Physics, University of Basel, Klingelbergstrasse 82, CH-4056 Basel, Switzerland

(Received 16 May 2025; revised 15 September 2025; accepted 19 December 2025; published 12 January 2026)

We investigate low-frequency noise in a spin-qubit device made in isotopically purified Si/Si-Ge. Observing sizable cross-correlations among energy fluctuations of different qubits, we conclude that these fluctuations are dominated by charge noise. At low frequencies, the noise spectra are not well described by a power law; instead, they reveal the presence of a few individual two-level fluctuators (TLFs). We demonstrate that the noise cross-correlations allow one to get information on the spatial location of such individual TLFs.

DOI: 10.1103/glp5-bb5b

Introduction—Charge noise is one of the major factors limiting the performance of solid-state quantum processors. The $1/f$-like power spectrum often observed at low frequencies is believed to arise from an ensemble of two-level fluctuators (TLFs) [1]. In silicon spin qubits, particularly those where the hyperfine noise is reduced by isotopic purification, the individual TLFs can sometimes be identified [2,3]. Recent work [4] has further shown that temperature and gate voltages can strongly affect the switching times of individual TLFs.

Despite extensive research, the precise nature of TLFs remains elusive [5]. Various suggestions predict TLFs located inside oxides, at interfaces [6,7], or at the quantum well [8]. In bare wafers, one can look for TLFs and impurities by direct imaging methods, such as atomic force microscopy; for example, the in-plane locations of TLFs at the Si/SiO_2 interface were traced in Ref. [9], and the 2DEG potential was mapped in Ref. [10]. However, for an actual nanodevice with a complex multilayer gate structure, direct imaging is difficult, and any hints on the spatial locations of TLFs causing qubit decoherence would be valuable.

In our recent works, we have developed [11] and applied [2,12] cross-power spectral densities (cross-PSDs) as a tool for the experimental study of noise in spin qubits [13]. The long-distance tails of noise correlations play a key role in quantum error correction [14,15]. At the same time, cross-correlations reveal temporal and spatial noise features that are absent in autocorrelations. In this Letter, we demonstrate that cross-PSDs can be used to estimate the spatial location of a TLF, on top of its characteristic switching time visible in the auto-PSDs.

The essence of the triangulation method—To explain the essence of the method, we start with the one-dimensional model of Ref. [12], describing two spin qubits coupled via exchange J in the device of Fig. 1. The external field $\mathbf{B}_{\mathrm{ext}}$ lies in the 2DEG plane along z, and a micromagnet provides the largest B_z gradient along the array axis x.

Charge-noise shifts the qubits within the plane. In the inhomogeneous field, these shifts induce Zeeman-energy noise,

$$\delta\nu_\alpha = \frac{g\mu_B}{h}\frac{\partial B_z}{\partial x}\delta x_\alpha, \tag{1}$$

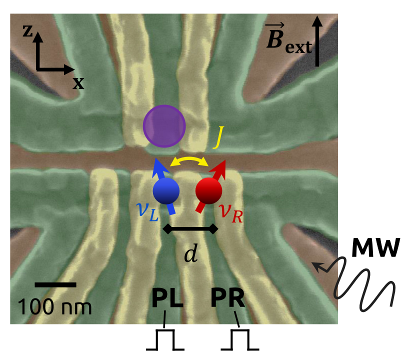

FIG. 1. Image of a device identical to the one measured. Qubits, depicted as colored spheres with arrows, are formed under plunger gates PL and PR. The qubits are separated by distance d, have Zeeman energies $h\nu_L$ and $h\nu_R$, and interact via exchange hJ. The purple circle indicates the charge sensor.

*Contact author: juan.rojasarias@riken.jp
†Contact author: tarucha@riken.jp

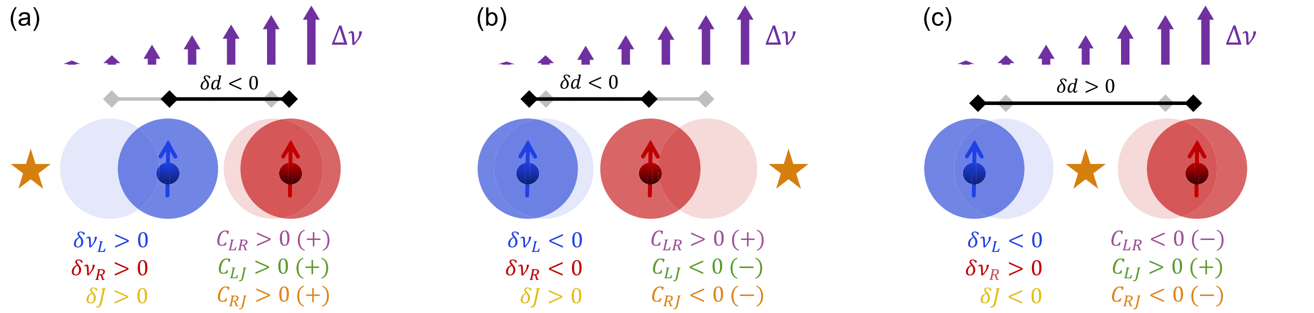

FIG. 2. Schematics of a TLF located (a) left, (b) right, or (c) between two qubits. The left (right) qubit is shown as a blue (red) arrow in a circle, and the TLF as a dark orange star. A purple gradient marks increasing qubit energies to the right, with the black line indicating qubit separation. Faint colors show positions before the $|0\rangle \to |1\rangle$TLF switch. Bottom panels display the resulting energy shifts and cross-PSD signs due to the TLF.

for qubit $\alpha \in L, R$, with δx_α the displacement along x, h Planck's constant, μ_B Bohr's magneton, and g the electron g factor. We assume (i) $\partial B_z/\partial x$ is positive and equal for both qubits, (ii) other magnetic gradients are negligible, (iii) the two dots' in-plane confinements are similar, and (iv) the dots operate at the charge symmetry point [16,17]. These assumptions are motivated by the device or serve only to simplify the presentation.

At the symmetry point, exchange fluctuations depend only on interdot tunneling, and hence a function of the interdot separation $d = x_R - x_L$. To lowest order, we have

$$\delta J = \frac{\partial J}{\partial d}(\delta x_R - \delta x_L). \tag{2}$$

Equations (1) and (2) allow us to relate exchange PSDs to qubit-energy PSDs, via

$$S_J(f) = \left(\frac{\partial J}{\partial \Delta}\right)^2 [S_L(f) + S_R(f) - 2\mathfrak{Re}C_{LR}(f)], \tag{3a}$$

$$C_{LJ}(f) = -\frac{\partial J}{\partial \Delta}[S_L(f) - C_{LR}(f)], \tag{3b}$$

$$C_{RJ}(f) = \frac{\partial J}{\partial \Delta}[S_R(f) - C^*_{LR}(f)]. \tag{3c}$$

with $\Delta = \nu_R - \nu_L$. We have denoted an auto-PSD by $S_\beta(f)$ and a cross-PSD by $C_{\beta\beta'}(f)$, with shorthands $\nu_\beta \to \beta$ for the PSD indexes of quantities $\beta \in \{\nu_L, \nu_R, J\}$. Thus, out of the six *a priori* independent PSDs for $\{\nu_L, \nu_R, J\}$, three are eliminated by Eq. (3).

To explain how a noise source location can be inferred from cross-PSDs, we look at three scenarios drawn in Fig. 2, with a TLF to the left, in between, or to the right of the qubits. While a TLF could in principle lie anywhere perpendicular to the qubit axis, here we focus on its position along the axis, assuming the magnetic-field gradient is dominant there and neglecting perpendicular contributions. We label the TLF states so that $|1\rangle$ electrostatically repels the qubits more than $|0\rangle$. We analyze the $|0\rangle \to |1\rangle$ transition, noting that the cross-PSD signs are unchanged for the reverse process and thus independent of labeling. We also assume the TLF acts instantaneously on both qubits, making all cross-PSDs real, as observed experimentally [2,12,18].

First, let us take a TLF located left of the array, Fig. 2(a). The TLF switch $|0\rangle \to |1\rangle$ pushes qubits to the right and, with a positive magnetic gradient, both qubit energies increase. The left qubit shifts slightly more, since it is closer to the TLF. Hence, the interdot separation decreases and the exchange goes up. In summary, all three quantities increase, and all three cross-PSDs are positive.

Second, consider a TLF located to the right of the array, Fig. 2(b). The TLF switch pushes the qubits in the opposite direction, and their energies decrease. The interdot distance still drops, in the same way as in the previous scenario. In summary, the two qubit energies are positively correlated, while each of them is negatively correlated with exchange.

Finally, consider a TLF inside the array, in between the two dots. The TLF switch pushes the dots apart, decreasing the left qubit energy while increasing the right qubit energy. Also, only in this case the interdot distance increases and the exchange energy drops. These changes result in the cross-correlations as given in Fig. 2(c).

A quantum device is typically influenced by many TLFs with different switching times and random locations, whose additive effects are hard to disentangle. Still, individual TLFs can sometimes be identified in the spectra as single Lorentzian contributions, from which their switching times are extracted. The procedure above goes further by also revealing their spatial location, providing information inaccessible from auto-PSDs alone.

Experimental demonstration—We demonstrate the method on data from the device in Fig. 1, previously used in Refs. [2,19]. It implements a triple quantum dot with aluminum gates over isotopically purified Si/Si-Ge (800 ppm ^{29}Si), where we operate only the two dots under PL and PR as single-electron spin qubits. We obtain time traces of ν_L, ν_R, and J via repeated interleaved Ramsey

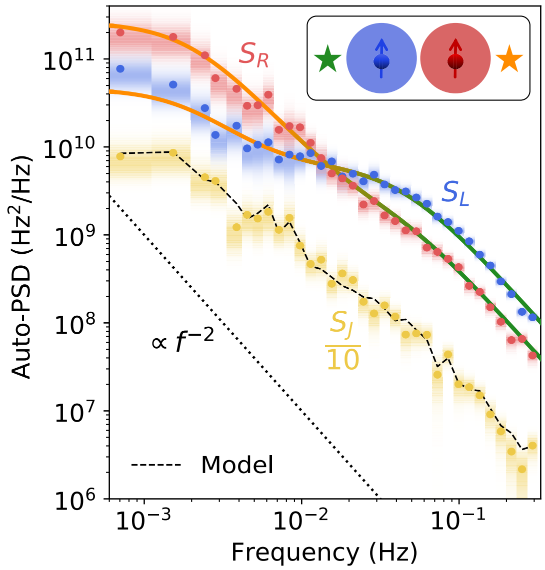

FIG. 3. Auto-PSDs of S_L (blue), S_R (red), and S_J (yellow). Color gradients show Bayesian probability distributions [11], with means as points. S_J is shifted down by a factor 10 for clarity. The black dashed line is the model prediction from Eq. (3). Gradient-colored fits of $S_L(f)$ and $S_R(f)$ use two Lorentzians $\propto [1 + 4\pi^2 f^2 \tau^2]^{-1}$ (see SM), with switching times $\tau = 3.7$ s (green) and $\tau = 90$ s (orange). A dotted line shows an f^{-2} dependence for reference.

experiments [12]. In Supplemental Material (SM) [20], we provide details on the experiment and data analysis.

Looking at the auto-PSDs in Fig. 3, two facts stand out: $S_L(f)$ and $S_R(f)$ have different shapes, and neither follows a simple $1/f$ law. These observations suggest that the noise arises from a few local sources near the qubits rather than from a global property. Indeed, the features can be captured by only two dominant TLFs, whose contributions appear as individual Lorentzians (solid lines), consistent with previous reports [2–4]. As we show next, the same two TLFs also reproduce the structure of the cross-PSDs, providing a unified picture of correlated noise. The SM presents the full set of fits, including all auto- and cross-PSDs.

To quantify correlations, we use cross-PSDs normalized by the auto-PSDs, $c_{\alpha\beta}(f) = C_{\alpha\beta}(f)/\sqrt{S_\alpha(f)S_\beta(f)}$. Each is a complex number with magnitude between 0 (uncorrelated) and 1 (perfectly correlated) and a phase. Figures 4(a) and 4(b) show the magnitudes and phases for qubit-qubit correlations. The correlations exceed 50% across most frequencies and reach over 90% at some points. The phase is zero everywhere, allowing us to exclude the scenario of Fig. 2(c). Thus, the two dominant TLFs in Fig. 3 are located outside the dot array.

We next examine correlations between qubit energies and exchange, shown in Figs. 4(c)–4(f). The magnitudes of $c_{LJ}(f)$ and $c_{RJ}(f)$ often exceed 80%. Since exchange arises purely from wave function overlap, such strong correlations demonstrate that the qubit-energy fluctuations have an electrical origin. This agrees with earlier results in Si/Si-Ge qubits [2–4,12], and contrasts with Si/SiO_2 devices where the relevant TLFs are individual nuclear spins [29–31]. We further test consistency with Eq. (3), with the dashed lines in Figs. 3 and 4 showing predictions obtained without free parameters, using $\partial J/\partial\Delta = -0.87$ extracted independently from J and Δ fluctuations (see SM). The excellent agreement confirms our noise model [Eq. (1)] and shows that individual TLFs can be resolved in both time traces and PSDs, enabling the classification of Fig. 2.

The phases of the three cross-PSDs, shown in the bottom row of Fig. 4, reveal three regions. For $f < 6$ mHz, they match Fig. 2(b), indicating a TLF to the right of the array, consistent with the stronger noise of the right qubit in Fig. 3. For $f > 40$ mHz, they correspond to Fig. 2(a), with a TLF to the left, again corroborated by stronger noise in the left qubit. A two-TLF fit (see SM) assigns switching times of 90 s and 3.7 s to these fluctuators, respectively. The intermediate region, $6 \leq f \leq 40$ mHz, reflects comparable effects of both TLFs and is a transition regime; the observed phases do not correspond to any scenario in Fig. 2.

Discussion—We now discuss our results focusing on applicability and limitations. In particular, we (i) apply our method to an independent dataset, (ii) consider extensions to larger arrays, (iii) examine refined triangulation through microscopic TLF models, (iv) outline potential problems, and (v) discuss other spin-qubit encodings.

First, to assess its generality, we apply our method to data obtained in Ref. [12] (natural silicon device with a different gate layout). The analysis (shown in SM) reveals two TLFs, one of which is positioned between the qubits [Fig. 2(c)], the other to the left. Including these data, we thus observe all three scenarios of Fig. 2 across four detectable TLFs, suggesting that each scenario occurs frequently.

Second, our analysis naturally extends to larger qubit arrays [32], as we show in simulations. For two qubits, correlations with exchange were needed to distinguish whether a TLF lies to the left or right of the qubits. In larger arrays, qubit-qubit energy correlations alone suffice, eliminating the need for exchange correlations and improving scalability. An illustrative case is shown in Fig. 5(a) for a 3×3 lattice. Knowing the magnetic-field profile, the analysis of Fig. 2 generalizes to two dimensions (see SM), where the plane divides into regions with distinct cross-PSD signatures, yielding a "tangram"like tiling [Fig. 5(a)]. Once a clear TLF signature is identified, its position is restricted to one such region.

Third, we turn to refined triangulation based on microscopic modeling. At this stage it is useful to separate two levels of localization: from the signs of the cross-PSDs we obtain a qualitative classification that places a TLF relative to the array [Figs. 2 and 5(a)], whereas extracting quantitative positions or absolute distances requires a model for the microscopic nature of the defect. If the spatial scaling of

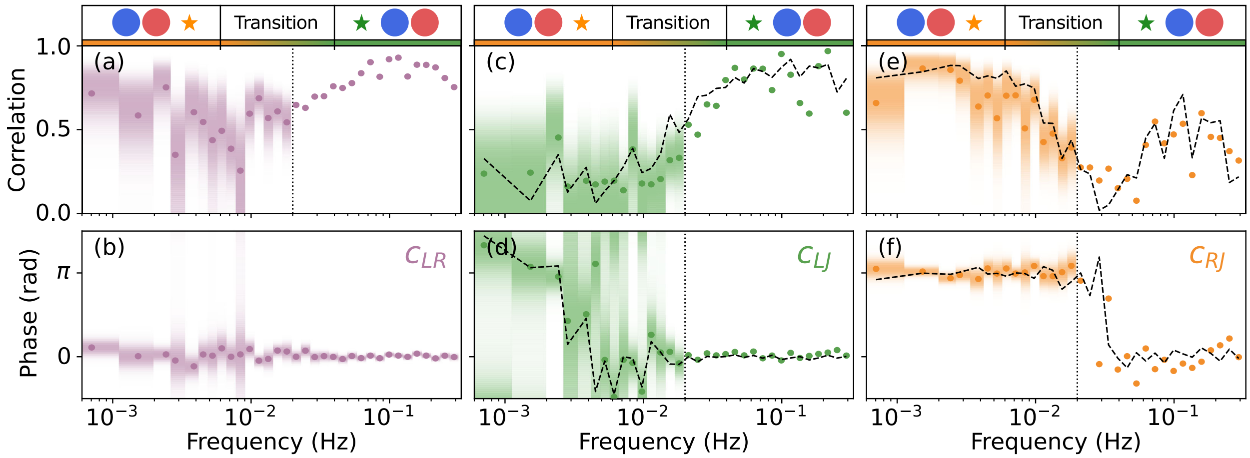

FIG. 4. Normalized cross-PSDs for the two-qubit system: c_{LR} (purple), c_{LJ} (green), and c_{RJ} (orange). Magnitudes are shown in (a),(c), (e) and phases in (b),(d),(f). Color gradients give Bayesian probability distributions with means as points. Vertical dotted lines mark the frequency above which spectra are corrected for estimation errors (see SM); only the phase of c_{LR} requires no correction. Black dashed lines are predictions from Eq. (3). Schematics indicate the dominant TLF regime: right of the qubits at low frequencies, left at high, and a transition in between.

the TLF-qubit interaction were known, finding the qubit-TLF coupling g^{α} for several qubits could, in principle, reveal the TLF's position. Even though measurement uncertainties usually limit such pinpointing, for the sake of illustration, we revisit the approach of Ref. [2] and model TLFs as charge traps in the oxide above the 2DEG, screened by a nearby metal. The $|0\rangle \rightarrow |1\rangle$ transition corresponds to trapping an elementary charge, equivalent to a dipole oriented perpendicular to the 2DEG. This model narrows the possible locations, illustrated in Fig. 5(b) for the 90 s TLF (see SM). Namely, the qubit-TLF couplings obtained from the PSD fits locate the TLF to the intersection of the solid curves (contours of constant qubit-energy shifts), yielding six candidate positions. The qualitative classification from cross-PSD signs (Fig. 2) excludes four and thus reveals that the TLF is horizontally about 100 nm from the qubit-array center. Nevertheless, we stress that extracted positions are sensitive to modeling assumptions. They depend on whether the TLF is an elementary charge or dipole, its distance to the 2DEG and screening metal, and the dipole's size and orientation. Without detailed knowledge or well-justified assumptions, absolute localization thus remains elusive. On the other hand, the same sensitivity helps narrow down the TLF model, as it should consistently describe spectra measured for multiple qubits simultaneously.

Fourth, we address possible ambiguities in interpreting cross-PSDs. In the previous paragraph, we considered a dipolar TLF with its charge dipole pointing out of the 2DEG plane. Were it oriented along the array axis, its effects would be more complex. For example, if located between the qubits, a TLF-state switch could attract one qubit while repelling the other, producing signatures that mimic a TLF pointing out of the plane located on either side of the array. Nevertheless, this ambiguity could be resolved by examining neighboring qubits, since their coupling strengths would differ strongly depending on the true TLF location. In contrast, a negative qubit-qubit cross-PSD, $C_{LR}(f) < 0$ (observed in the SM), can only arise from a TLF between the qubits and is therefore a robust signature of such scenario. A similar ambiguity arises when the dots' in-plane confinements strongly differ. Then, a TLF switch could displace the loosely bound dot more, even if it is farther from the TLF. However, such asymmetry would yield smaller noise in the tightly bound dot, inconsistent with the crossover between S_L and S_R in Fig. 3. Finally, we consider the case of two (or more) TLFs having similar switching times. Their Lorentzian spectra overlap and, in two-qubit data, cannot be distinguished from a single TLF. Data from larger arrays, however, could help identify individual TLFs by their distinct spatial correlation patterns. We conclude with a somewhat obvious statement: the more precisely the dots and TLFs are characterized, the more reliable the classification of Fig. 2 and associated PSD fits will be.

Finally, we comment on the broader applicability of our approach to other spin-qubit encodings. Although we focused on electron spins in micromagnet-induced gradients, the same principles apply to other spin-qubit encodings. For hole spin qubits in germanium, anisotropic g tensors replace engineered gradients; once the g-tensor axes are known, the tangramlike classification of Fig. 5(a) can be constructed and TLFs localized from cross-PSD signs. A similar strategy applies to singlet-triplet or exchange-only (EO) qubits, using cross-PSDs of exchange interactions. For example, in a linear EO qubit formed by three spins with intraqubit couplings J_{12} and J_{23}, a TLF on either side of the array yields positive correlations between

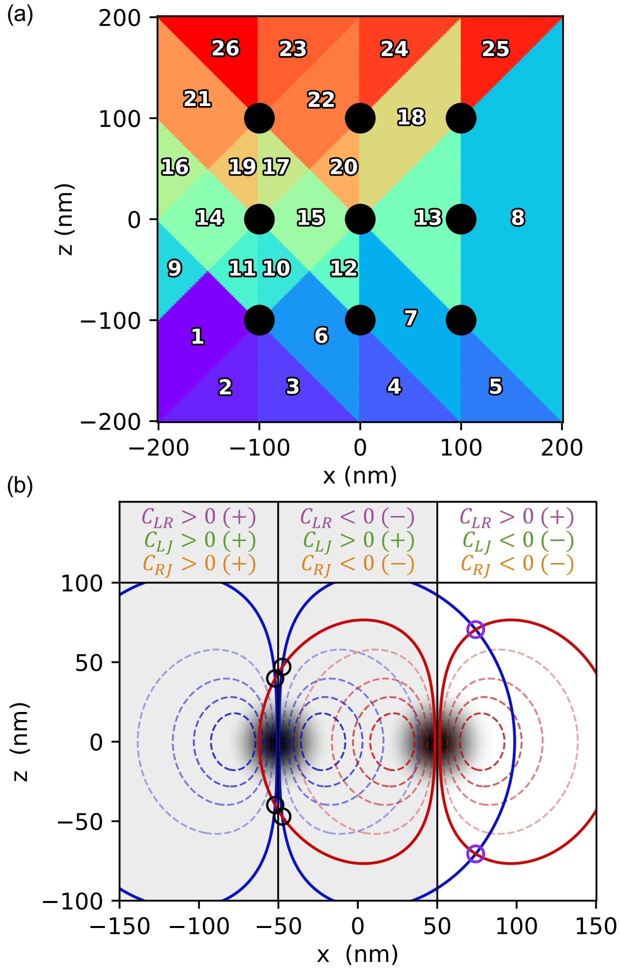

FIG. 5. TLF triangulation in two dimensions. (a) Regions with distinct cross-PSD signatures for a 3×3 qubit array (black circles). The tiling corresponds to a magnetic gradient $\nabla B_z \propto 1\hat{x} - 0.1z\hat{z}$, similar to that of the device in Fig. 1 [2]. Analogous tilings can be constructed for any known magnetic profile (or spin-orbit axis or g tensor). (b) Contours of qubit-TLF interaction strength for a screened charge trap [2]. Qubit wave functions are shown as Gaussian profiles (20 nm width). Dashed blue (red) lines denote contours of constant energy shifts for the left (right) qubit; solid lines match fitted jumps from PSD analysis ($|g^L| = 14.9$ kHz, $|g^R| = 38.0$ kHz, for the 90 s TLF). Intersections mark six candidate positions, with cross-PSD signs excluding the gray region and only leaving two possible locations (purple circles).

the two exchanges, while one inside gives negative correlations. Interqubit couplings to neighboring qubits, or triangular EO geometries with additional intraqubit coupling J_{13} [33], could provide extra constraints to further refine localization. Either way, EO qubit lattices map onto tangramlike patterns of exchange cross-PSD signs (see SM), providing a general framework to infer TLF positions.

Conclusions—Using two spin qubits in an isotopically purified Si/Si-Ge device, we have investigated noise cross-correlations between the qubit Zeeman energies and between the qubit energies and exchange energy, finding them consistent with charge TLFs located near the qubits. We introduced a simple classification where the signs of the three cross-PSDs reveal the spatial location of dominant TLFs and their characteristic times. In our device, we identified one TLF to the left of the array with a switching time of 3.7 s and another to the right with a switching time of 90 s. Extending the method to two dimensions, we constructed tiling plots that divide real space into regions with distinct cross-PSD signatures. This framework provides a systematic way to classify possible TLF locations in larger qubit arrays and generalizes naturally to other spin-qubit encodings.

Acknowledgments—This work was supported by the Swiss National Science Foundation and NCCR SPIN Grant No. 51NF40-180604, JST Moonshot R&D Grants No. JPMJMS226B and No. JPMJMS2065, JSPS KAKENHI Grants No. JP23H01790 and No. JP23H05455. J. S. R.-A. acknowledges support from the Gutaiteki Collaboration Seed, and J. Y. support from The Precise Measurement Technology Promotion Foundation and The Nakajima Foundation. We also acknowledge support from JST PRESTO Grants No. JPMJPR23F8 (A. N.), No. JPMJPR2017 (T. N.), and No. JPMJPR21BA (J. Y.).

Data availability—The data that support the findings of this article are openly available [34].

[1] J. Bernamont, Fluctuations de potentiel aux bornes d'un conducteur métallique de faible volume parcouru par un courant, Ann. Phys. (Berlin) **11**, 71 (1937).

[2] J. S. Rojas-Arias, A. Noiri, P. Stano, T. Nakajima, J. Yoneda, K. Takeda, T. Kobayashi, A. Sammak, G. Scappucci, D. Loss, and S. Tarucha, Spatial noise correlations beyond nearest neighbors in ^{28}Si/Si-Ge spin qubits, Phys. Rev. Appl. **20**, 054024 (2023).

[3] E. J. Connors, J. Nelson, L. F. Edge, and J. M. Nichol, Charge-noise spectroscopy of Si/SiGe quantum dots via dynamically-decoupled exchange oscillations, Nat. Commun. **13**, 940 (2022).

[4] F. Ye, A. Ellaboudy, D. Albrecht, R. Vudatha, N. T. Jacobson, and J. M. Nichol, Characterization of individual charge fluctuators in Si/SiGe quantum dots, Phys. Rev. B **110**, 235305 (2024).

[5] C. Müller, J. H. Cole, and J. Lisenfeld, Towards understanding two-level-systems in amorphous solids: Insights from quantum circuits, Rep. Prog. Phys. **82**, 124501 (2019).

[6] E. J. Connors, J. J. Nelson, H. Qiao, L. F. Edge, and J. M. Nichol, Low-frequency charge noise in Si/SiGe quantum dots, Phys. Rev. B **100**, 165305 (2019).

[7] A. V. Kuhlmann, J. Houel, A. Ludwig, L. Greuter, D. Reuter, A. D. Wieck, M. Poggio, and R. J. Warburton, Charge noise and spin noise in a semiconductor quantum device, Nat. Phys. **9**, 570 (2013).

[8] B. Paquelet Wuetz, D. Degli Esposti, A.-M. J. Zwerver, S. V. Amitonov, M. Botifoll, J. Arbiol, A. Sammak, L. M. K. Vandersypen, M. Russ, and G. Scappucci, Reducing charge noise in quantum dots by using thin silicon quantum wells, Nat. Commun. **14**, 1385 (2023).

[9] M. Cowie, P. C. Constantinou, N. J. Curson, T. J. Z. Stock, and P. Grütter, Spatially resolved random telegraph fluctuations of a single trap at the Si/SiO_2 interface, Proc. Natl. Acad. Sci. U.S.A. **121**, e2404456121 (2024).

[10] M. A. Topinka, B. J. LeRoy, R. M. Westervelt, S. E. J. Shaw, R. Fleischmann, E. J. Heller, K. D. Maranowski, and A. C. Gossard, Coherent branched flow in a two-dimensional electron gas, Nature (London) **410**, 183 (2001).

[11] Á. Gutiérrez-Rubio, J. S. Rojas-Arias, J. Yoneda, S. Tarucha, D. Loss, and P. Stano, Bayesian estimation of correlation functions, Phys. Rev. Res. **4**, 043166 (2022).

[12] J. Yoneda, J. S. Rojas-Arias, P. Stano, K. Takeda, A. Noiri, T. Nakajima, D. Loss, and S. Tarucha, Noise-correlation spectrum for a pair of spin qubits in silicon, Nat. Phys. **19**, 1793 (2023).

[13] M. B. Donnelly, J. Rowlands, L. Kranz, Y. L. Hsueh, Y. Chung, A. V. Timofeev, H. Geng, P. Singh-Gregory, S. K. Gorman, J. G. Keizer, R. Rahman, and M. Y. Simmons, Noise correlations in an atom-based quantum dot array, Phys. Rev. Appl. **23**, 064058 (2025).

[14] B. D. Clader, C. J. Trout, J. P. Barnes, K. Schultz, G. Quiroz, and P. Titum, Impact of correlations and heavy tails on quantum error correction, Phys. Rev. A **103**, 052428 (2021).

[15] J. P. Clemens, S. Siddiqui, and J. Gea-Banacloche, Quantum error correction against correlated noise, Phys. Rev. A **69**, 062313 (2004).

[16] F. Martins, F. K. Malinowski, P. D. Nissen, E. Barnes, S. Fallahi, G. C. Gardner, M. J. Manfra, C. M. Marcus, and F. Kuemmeth, Noise suppression using symmetric exchange gates in spin qubits, Phys. Rev. Lett. **116**, 116801 (2016).

[17] M. D. Reed, B. M. Maune, R. W. Andrews, M. G. Borselli, K. Eng, M. P. Jura, A. A. Kiselev, T. D. Ladd, S. T. Merkel, I. Milosavljevic, E. J. Pritchett, M. T. Rakher, R. S. Ross, A. E. Schmitz, A. Smith, J. A. Wright, M. F. Gyure, and A. T. Hunter, Reduced sensitivity to charge noise in semiconductor spin qubits via symmetric operation, Phys. Rev. Lett. **116**, 110402 (2016).

[18] J. S. Rojas-Arias, Y. Kojima, K. Takeda, P. Stano, T. Nakajima, J. Yoneda, A. Noiri, T. Kobayashi, D. Loss, and S. Tarucha, The origins of noise in the zeeman splitting of spin qubits in natural-silicon devices, npj Quantum Inf. 10.1038/s41534-025-01150-6 (2025).

[19] A. Noiri, K. Takeda, T. Nakajima, T. Kobayashi, A. Sammak, G. Scappucci, and S. Tarucha, Fast universal quantum gate above the fault-tolerance threshold in silicon, Nature (London) **601**, 338 (2022).

[20] See Supplemental Material at http://link.aps.org/supplemental/10.1103/glp5-bb5b for details on the experiments, the protocol for correction of PSDs, the reproduction of cross-PSDs from Ref. [12], the model of TLF-qubit coupling, and the tiling of space in regions with unique cross-PSD characteristics. It also includes Refs. [21–28].

[21] A. Noiri, K. Takeda, J. Yoneda, T. Nakajima, T. Kodera, and S. Tarucha, Radio-frequency-detected fast charge sensing in undoped silicon quantum dots, Nano Lett. **20**, 947 (2020).

[22] J. M. Elzerman, R. Hanson, L. H. Willems van Beveren, B. Witkamp, L. M. K. Vandersypen, and L. P. Kouwenhoven, Single-shot read-out of an individual electron spin in a quantum dot, Nature (London) **430**, 431 (2004).

[23] K. Takeda, J. Kamioka, T. Otsuka, J. Yoneda, T. Nakajima, M. R. Delbecq, S. Amaha, G. Allison, T. Kodera, S. Oda, and S. Tarucha, A fault-tolerant addressable spin qubit in a natural silicon quantum dot, Sci. Adv. **2**, e1600694 (2016).

[24] M. R. Delbecq, T. Nakajima, P. Stano, T. Otsuka, S. Amaha, J. Yoneda, K. Takeda, G. Allison, A. Ludwig, A. D. Wieck, and S. Tarucha, Quantum dephasing in a gated GaAs triple quantum dot due to nonergodic noise, Phys. Rev. Lett. **116**, 046802 (2016).

[25] T. Nakajima, A. Noiri, K. Kawasaki, J. Yoneda, P. Stano, S. Amaha, T. Otsuka, K. Takeda, M. R. Delbecq, G. Allison, A. Ludwig, A. D. Wieck, D. Loss, and S. Tarucha, Coherence of a driven electron spin qubit actively decoupled from quasistatic noise, Phys. Rev. X **10**, 011060 (2020).

[26] J. Lisenfeld, A. Bilmes, S. Matityahu, S. Zanker, M. Marthaler, M. Schechter, G. Schön, A. Shnirman, G. Weiss, and A. V. Ustinov, Decoherence spectroscopy with individual two-level tunneling defects, Sci. Rep. **6**, 23786 (2016).

[27] L. C. Camenzind, L. Yu, P. Stano, J. D. Zimmerman, A. C. Gossard, D. Loss, and D. M. Zumbühl, Spectroscopy of quantum dot orbitals with in-plane magnetic fields, Phys. Rev. Lett. **122**, 207701 (2019).

[28] V. John, C. X. Yu, B. van Straaten, E. A. Rodríguez-Mena, M. Rodríguez, S. D. Oosterhout, L. E. A. Stehouwer, G. Scappucci, M. Rimbach-Russ, S. Bosco, F. Borsoi, Y.-M. Niquet, and M. Veldhorst, Robust and localised control of a 10-spin qubit array in germanium, Nat. Commun. **16**, 10560 (2025).

[29] R. Zhao, T. Tanttu, K. Y. Tan, B. Hensen, K. W. Chan, J. C. C. Hwang, R. C. C. Leon, C. H. Yang, W. Gilbert, F. E. Hudson, K. M. Itoh, A. A. Kiselev, T. D. Ladd, A. Morello, A. Laucht, and A. S. Dzurak, Single-spin qubits in isotopically enriched silicon at low magnetic field, Nat. Commun. **10**, 5500 (2019).

[30] B. Hensen, W. Wei Huang, C.-H. Yang, K. Wai Chan, J. Yoneda, T. Tanttu, F. E. Hudson, A. Laucht, K. M. Itoh, T. D. Ladd, A. Morello, and A. S. Dzurak, A silicon quantum-dot-coupled nuclear spin qubit, Nat. Nanotechnol. **15**, 13 (2020).

[31] W. Huang, C. H. Yang, K. W. Chan, T. Tanttu, B. Hensen, R. C. C. Leon, M. A. Fogarty, J. C. C. Hwang, F. E. Hudson, K. M. Itoh, A. Morello, A. Laucht, and A. S. Dzurak, Fidelity benchmarks for two-qubit gates in silicon, Nature (London) **569**, 532 (2019).

[32] S. G. J. Philips, M. T. Madzik, S. V. Amitonov, S. L. de Snoo, M. Russ, N. Kalhor, C. Volk, W. I. L. Lawrie, D. Brousse, L. Tryputen, B. P. Wuetz, A. Sammak, M. Veldhorst, G. Scappucci, and L. M. K. Vandersypen, Universal control of a six-qubit quantum processor in silicon, Nature (London) **609**, 919 (2022).

[33] E. Acuna, J. D. Broz, K. Shyamsundar, A. B. Mei, C. P. Feeney, V. Smetanka, T. Davis, K. Lee, M. D. Choi, B. Boyd, J. Suh, W. Ha, C. Jennings, A. S. Pan, D. S. Sanchez, M. D. Reed, and J. R. Petta, Coherent control of a triangular

exchange-only spin qubit, Phys. Rev. Appl. **22**, 044057 (2024).

[34] J. S. Rojas-Arias, A. Noiri, J. Yoneda, P. Stano, T. Nakajima, K. Takeda, G. Scappucci, S. Tarucha, and D. Loss, Data accompanying the publication “Inferring charge noise source locations from correlations in spin qubits”, 10.5281/zenodo.18013360 (2025).